Supplementary Information

Programmable protein delivery from microgel/hydrogel composites (MHCs) via discrete combinations of multi-state protein-loaded unit ingredients

Longfei CHEN,*[a] and Saif A. Khan [b,c]

Contents

S.1. Chemical Syntheses and Characterizations

S.1.1. Vinylation of Polysaccharides (Dex_{40k}-VS & Dex_{40k}-$FITC_{1\%}$-VS)

The vinylation protocol in this study closely followed a report by Yu and Chau [1]. Briefly, 3.2 g Dex_{40k}-OH was dissolved in 10 mM NaOH (aq.) solution to a final concentration of 4.0 w/v%. Under room temperature and stirring, 9 mL DVS (1.5x functional group eqv. to hydroxyl) were injected into the solution rapidly, and the reaction was held for 3 min (or 5 min). Upon completion, the reaction was terminated by adding 1 M HCl (aq.) solution to lower pH down to ~4.5. Then, the reaction mixture was loaded into Pur-A-Lyzer™ Mega 3500 (Sigma-Aldrich, PURG35010) dialysis cassettes (regenerated cellulose, MWCO ~3.5 kDa) and dialyzed against 4.0 L Milli Q ultrapure water for at least 8 times (≥ 6.0 hrs each time). The dialyzed solution was frozen in -80 °C fridge overnight and lyophilized in vacuum freeze dryer for 3 days. The lyophilized pinkish white fibrous solid material was characterized using proton nuclear magnetic resonance spectroscopy (^{1}H NMR, 400 MHz) by dissolving in deuterium oxide (D_2O, Sigma-Aldrich 191701). Similarly, Dex_{40k}-$FITC_{1\%}$-OH was reacted following the identical procedures, and the lyophilized bright yellow fibrous solid material was similarly characterized by ^{1}H NMR in D_2O. The NMR spectra and determination of repeating-unit based degree of modification (DM) of Dex_{40k}-$VS_{5\%}$ (10 mM NaOH, reacted for 3 min), Dex_{40k}-$FITC_{1\%}$-$VS_{6\%}$ (10 mM NaOH, reacted for 3 min), and Dex_{40k}-$VS_{10\%}$ (10 mM NaOH, reacted for 5 min) were shown in **Fig. S1**.

Here, we calculate the repeating-unit based degree of modification (DM) by extracting the area of ^{1}H NMR peaks located at δ 4.9 ~ 5.3 (s, 1H) indicating the α-H of the ring-oxygen atom (potentially of different chemical environment due to branching and substitutions) which marks a single repeating unit, at δ 6.3 ~ 6.5 (m, 2H) indicating the α-H on C=C double bond of the sulfonyl group, and at δ 6.85 ~ 7.0 (m, 1H) indicating mixed peaks of the 2 terminal H atoms on C=C double bond of vinyl sulfonyl substitution. Hence, the DM is defined as the following **Eqn. S1**.

$$DM_{VS} = \frac{No.\ of\ vinyl\ substitution}{No.\ of\ repeating\ units} = \frac{area\ of\ peaks\ \delta\ 6.3 \sim 6.5}{area\ of\ peaks\ \delta\ 6.85 \sim 7.0} \times 100\% \qquad \textbf{Eqn. S1}$$

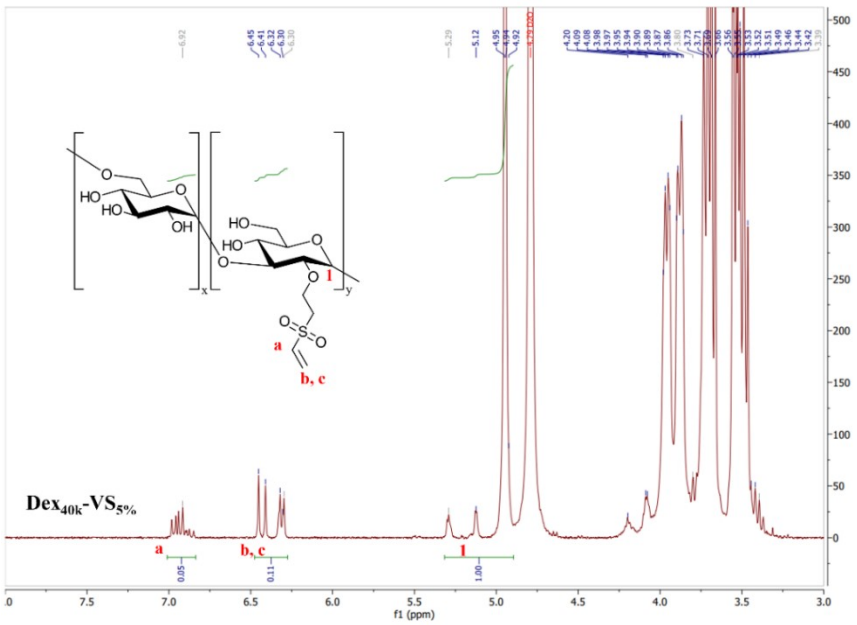

Figure S1A. ^{1}H NMR (Brunker 400 MHz) spectrum of Dex_{40k}-$VS_{5\%}$ in D_2O ($\delta_{solvent}$ = 4.79 ppm), with informative peaks: δ 4.9 ~ 5.3 (s, 1H), 6.3 ~ 6.5 (m, 2H), and 6.85 ~ 7.0 (m, 1H).

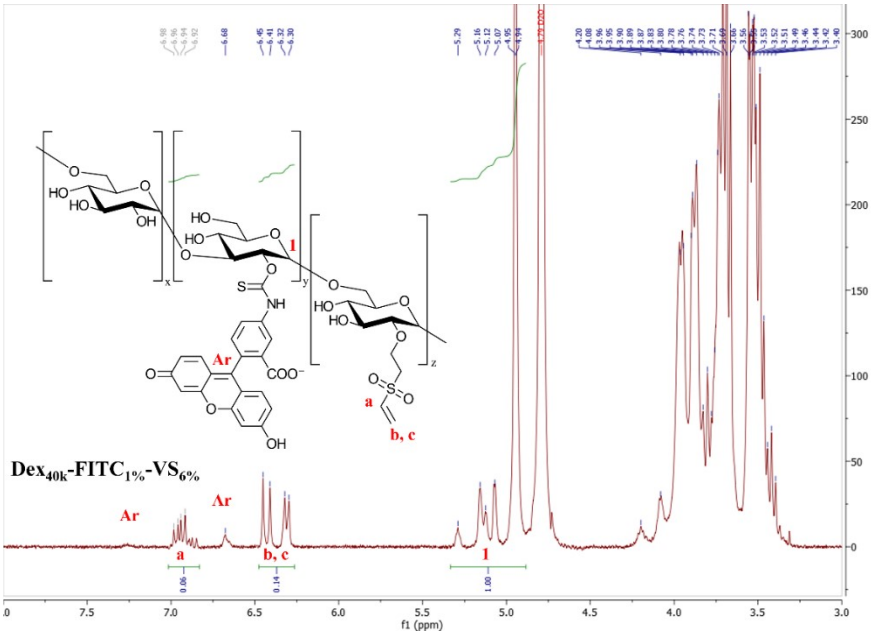

Figure S1B. ^{1}H NMR (Brunker 400 MHz) spectrum of Dex_{40k}-$FITC_{1\%}$-$VS_{6\%}$ in D_2O ($\delta_{solvent}$ = 4.79 ppm), with informative peaks: δ 4.9 ~ 5.3 (s, 1H), 6.3 ~ 6.5 (m, 2H), and 6.85 ~ 7.0 (m, 1H).

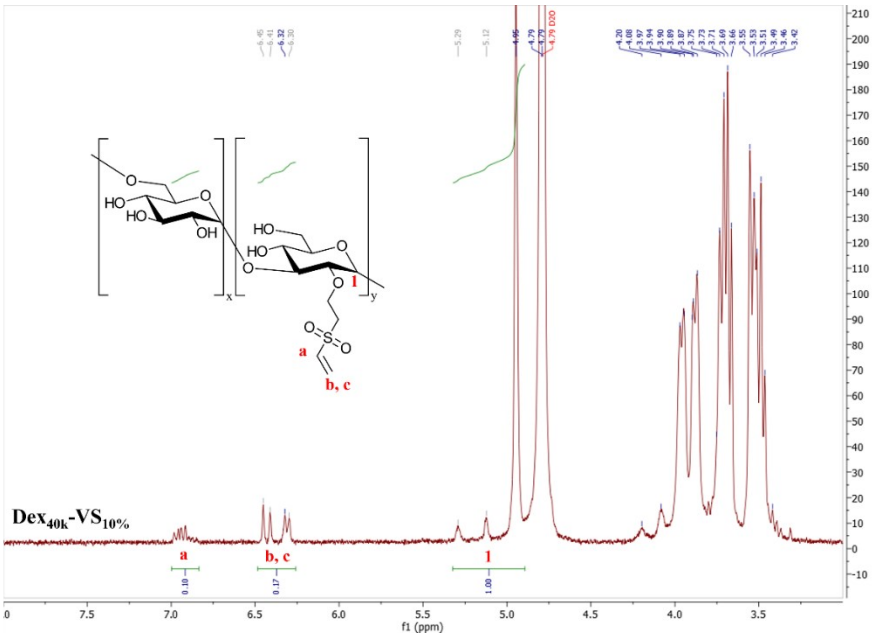

Figure S1C. ^{1}H NMR (Brunker 400 MHz) spectrum of Dex_{40k}-$VS_{10\%}$ in D_2O ($\delta_{solvent}$ = 4.79 ppm), with informative peaks: δ 4.9 ~ 5.3 (s, 1H), 6.3 ~ 6.5 (m, 2H), and 6.85 ~ 7.0 (m, 1H).

S.1.2. Thiolation of Vinylated Polysaccharides (Dex40k-SO2-TTSH)

The thiolation protocol for Dex-VS in this study was adopted from a work done by Chau and colleagues [2]. Briefly, 2.5 g Dex_{40k}-$VS_{10\%}$ was dissolved in 100 mM pH ~ 7.4 PB to a final concentration of 2.5 w/v%. The reaction mixture was then purged with dry pure nitrogen (N_2) for 30 min to remove dissolved oxygen. In a separate vial, 2.41 g DTT (10x functional group eqv. to vinylsulfone) were weighed and dissolved in 2.0 mL 100 mM pH ~ 7.4 PB and purged with dry pure N_2 for 5 min. Under room temperature and strong stirring, the DTT solution was injected into the reaction mixture rapidly, and the reaction was held for 5 hrs. Upon completion,

the reaction was terminated by adding 1.0 M HCl (aq.) solution to lower the pH down to approximately 4. Then, the reaction mixture was loaded into Pur-A-Lyzer™ Mega 3500 (Sigma-Aldrich, PURG35010) dialysis cassettes (regenerated cellulose, MWCO ~3.5 kDa) and dialyzed against 4.0 L dilute HCl solution (pH ~ 4) in Milli Q ultrapure water for at least 8 times (≥ 6.0 hrs each time). The dialyzed solution was frozen in -80 °C fridge overnight and lyophilized in vacuum freeze dryer for 72 hrs. The lyophilized white fibrous solid was characterized by Ellman's Assay to obtain the repeating-unit-based DM of Dex_{40k}-SO_2-$TTSH_{5.5\%}$.

Basically, 4.0 mg of Ellman's reagent, 5,5′-dithiobis-(2-nitrobenzoic acid) (DTNB), was first dissolved in 1.0 mL of pre-concocted Ellman's phosphate buffer (EPB) to a working concentration of 4.0 mg/mL. Next, a series of Dex_{40k}-SO_2-TTSH solution dissolved in EPB with known concentrations of 1.0, 0.5, 0.2 and 0.1 w/v % (with a blank reference of EPB) were sampled with 25 µL volume and loaded onto a clean 96-well Greiner polystyrene microplate (triplicated for each concentration), followed by addition of 5 µL of working DTNB solution and 250 µL diluting buffer to a final volume of 280 µL in each well. After incubation at room temperature with gentle shaking for 15 min, the absorbance of each mixed and fully developed sample was measured using Tecan® Infinite 200-Pro Plate Reader at λ = 412 nm. Assuming that the average molecular weight of dextran repeating unit, which is 160 Da, will not be much affected due to minor amount of substitution, the molar concentration of repeating units was computed by firstly converting the weight-over-volume percentage concentration of polymers into molar concentration, and secondly dividing the average molecular weight of repeating unit. Next, with referrable specifications of Greiner microplate (37.828 mm^2 cross-sectional area of a well), for a volume of 280 µL in each well, the mean light path (l) can be estimated to be 0.740 cm. Lastly, based on Beer-Lambert's Law with documented extinction coefficients of the reacted products of DTNB (ε = 14150 M^{-1} cm^{-1}), the molar concentration of available free thiol in sample was computed by following **Eqn. S2A**.

$$C_{SH} = \frac{(averaged\ absorbance\ @\ 412\ nm) - (averaged\ blank\ reference)}{\varepsilon \cdot l} \qquad \textbf{Eqn. S2A}$$

As a result, the repeating-unit-based degree of modification (DM) was computed by following **Eqn. S2B**.

$$DM_{SH} = \frac{C_{SH}}{molar\ concentration\ of\ R.U.} \qquad \textbf{Eqn. S2B}$$

Table S1. Collected absorbance data of Dex_{40k}-SO_2-TTSH Ellman's Assay and analysis.

Raw Data & Protocol									
Plate				Greiner 96 Flat Bottom Transparent Polystyrene Cat. No.: 655101/655161/655192 [GRE96ft.pdfx]					
Device				infinite 200Pro					
Mode				Absorbance					
Wavelength				412	nm				
Bandwidth				9	nm				
Number of Flashes				25					
Settle Time				0	ms				
	Temperature: 21.5 °C								
<>	1	2	3	4	8				
A	3.3222	1.6612	0.7269	0.4128	0.0884				
B	3.3442	1.6674	0.7108	0.4097	0.0799				
C	3.343	1.659	0.6945	0.4065	0.0761				
V =	5	uL (reagent) +		25	uL (sample) +	250	uL (buffer) =	280	uL
Analysis									
	1	2	3	4	8		Standard 96-well plate		
Conc. (w/v %)	1.000	0.500	0.200	0.100	0.000	Hw (flat-bottom) =	10.65	mm	
R.U. (mM)	62.500	31.250	12.500	6.250	0.000	Dw =	6.94	mm	
Avg. Abs. (A.U.)	3.336	1.663	0.711	0.410	0.081	Cross-sectional Area =	37.828	mm^2	
Avg. Abs. -bkg. (A.U.)	3.255	1.581	0.629	0.328	0.000				
S.D. Abs. (A.U.)	0.012	0.004	0.016	0.003	0.006	Light Path (L) =	0.740	cm	
free-thiol, by B-L (mM)	3.480674	1.690684	0.672895	0.350955	0	Distinction Coeff. (E) =	14150	M^(-1) * cm^(-1)	
DM, by B-L (%)	5.57%	5.41%	5.38%	5.62%	5.49%				

S.2. Hydrogel Formulation and Characterizations

S.2.1. Formulation of Microgels

As described in the main text, three types of microgels were fabricated: sol-nLyz, coa-nLyz, and sol-pBSA. For all formulations, a generic pair of Dex_{40k}-$VS_{5\%}$ and Dex_{40k}-SO_2-$TTSH_{5.5\%}$ was used to facilitate a thiol-ene Michael addition 'click chemistry' for crosslinking. As decided after several trial batches of fabrication, 8 w/v % of the total dextran concentration was determined to ensure gelation, manipulatable mechanical properties, dissolution kinetics, and reasonable swelling behavior. Notably, 8 % of the Dex_{40k}-$VS_{5\%}$ was replaced by Dex_{40k}-$FITC_{1\%}$-$VS_{6\%}$ for a visible and fluorescent color for visualization, and the final VS:SH ratio was kept at 1:1.2 for all formulations to ensure full consumption of reactive VS moieties. Specially, for coa-nLyz microgels, coacervating agents (Dex_{40k}-SO_3Na) were loaded into the hydrogel in free solute form, which would be able to co-release together with protein payload. This was considered not practically favorable due to the potential problem of biological activity and compatibility of Dex_{40k}-SO_3Na. Hence, in future studies, immobilizing coacervating agents or incorporating charges onto the crosslinked network will be applied to mitigate the uncertain biological effects arise from the coacervating agents while maintaining the hindrance from ionic interactions and coacervations. **Table S2** column 1 ~ 6 summarize the detailed formulations, and column 7 summarize a rough estimation of gelling time done by rheological monitoring of viscosity profile developed during gelation, as shown by following **Fig. S2**.

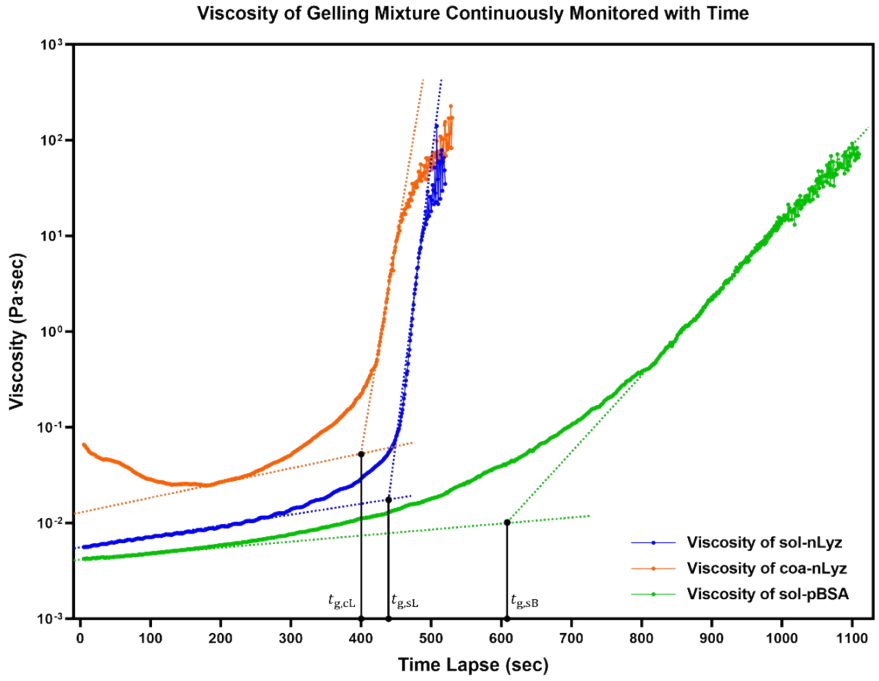

Figure S2. Rheological continuous monitoring of (logarithmic) viscosity of different formulation gelling mixtures over time. The inflection point between two linearly increasing stages were interpolated as the gelation time indicated in the plot.

S.2.2. Microscopic Sizing of Freshly Fabricated Microgels

As described in the main text, all 3 types of microgels were sized with ImageJ as the following **Fig. S3A**, **S3B**, and **S3C** with labelled diameters indicating each measurable microgels of sol-nLyz, coa-nLyz, and sol-pBSA, respectively. As a result, **Fig. S3D** box plot was generated to summarize the size distribution data, and **Table S2** column 8 summarize the average size of microgels.

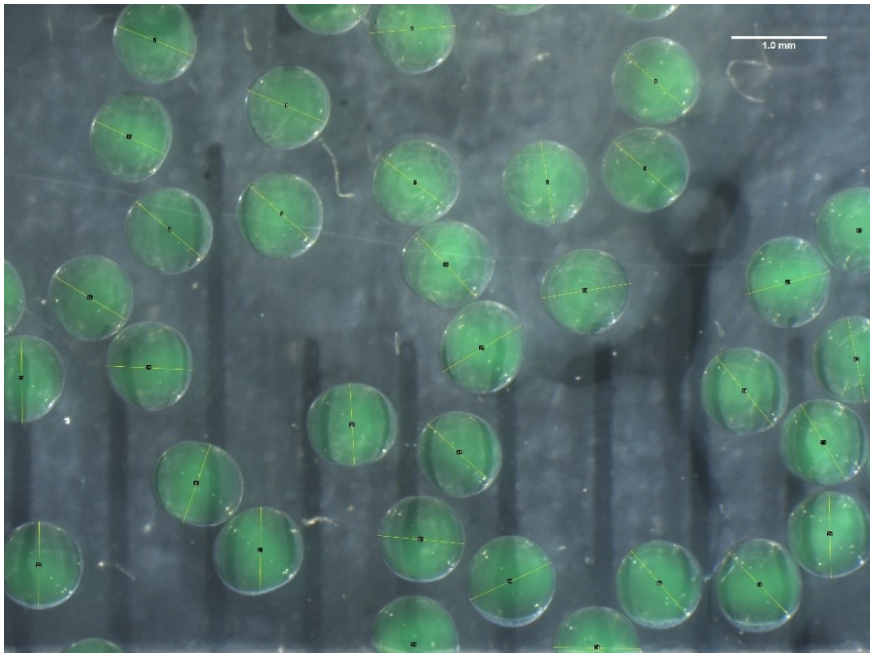

Figure S3A. Sample microscopic image of sampled sol-nLyz microgels processed for sizing. Yellow strikes indicate the manually chosen diameter for approximate measurements.

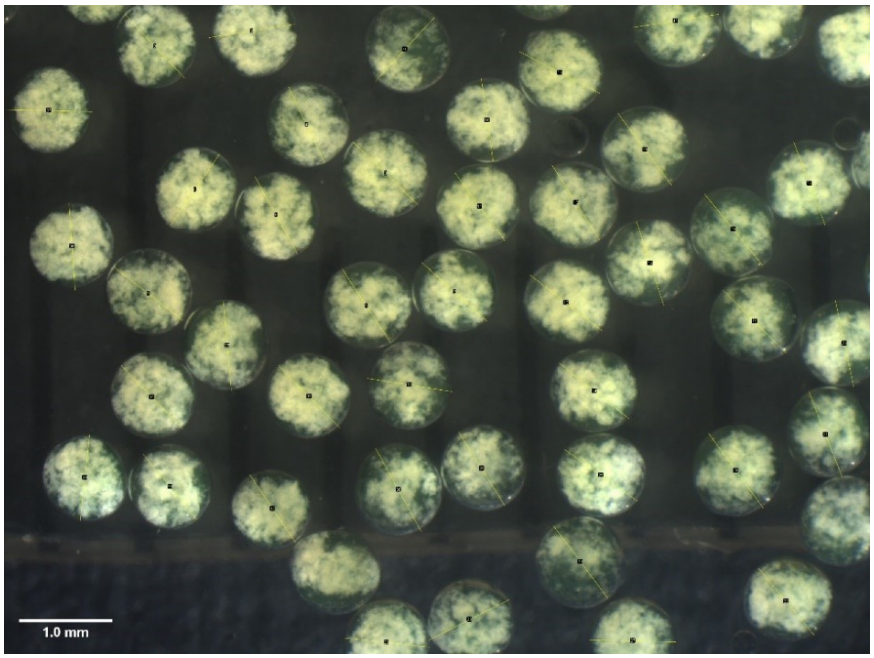

Figure S3B. Sample microscopic image of sampled coa-nLyz microgels processed for sizing. Yellow strikes indicate the manually chosen diameter for approximate measurements.

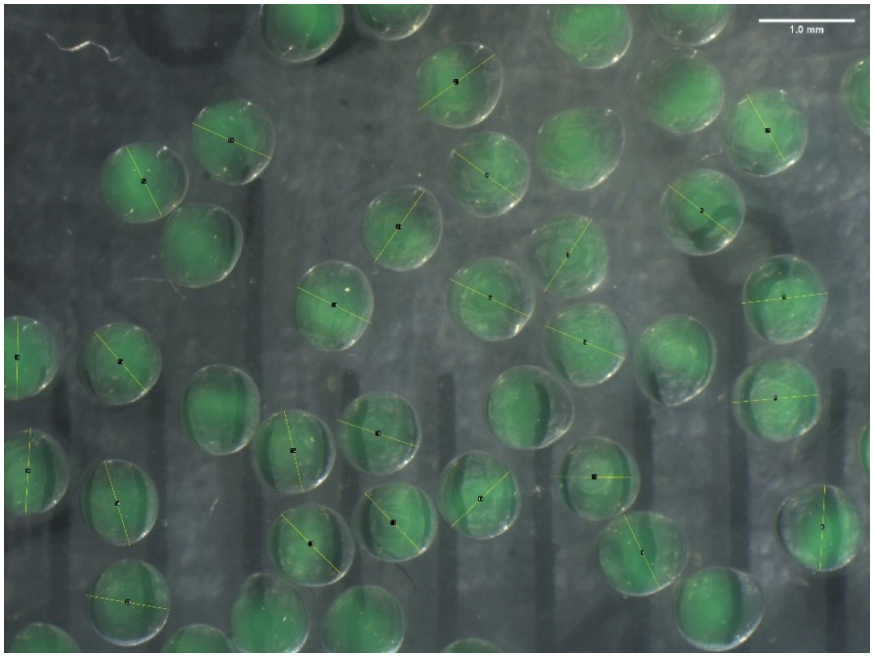

Figure S3C. Sample microscopic image of sampled sol-pBSA microgels processed for sizing. Yellow strikes indicate the manually chosen diameter for approximate measurements.

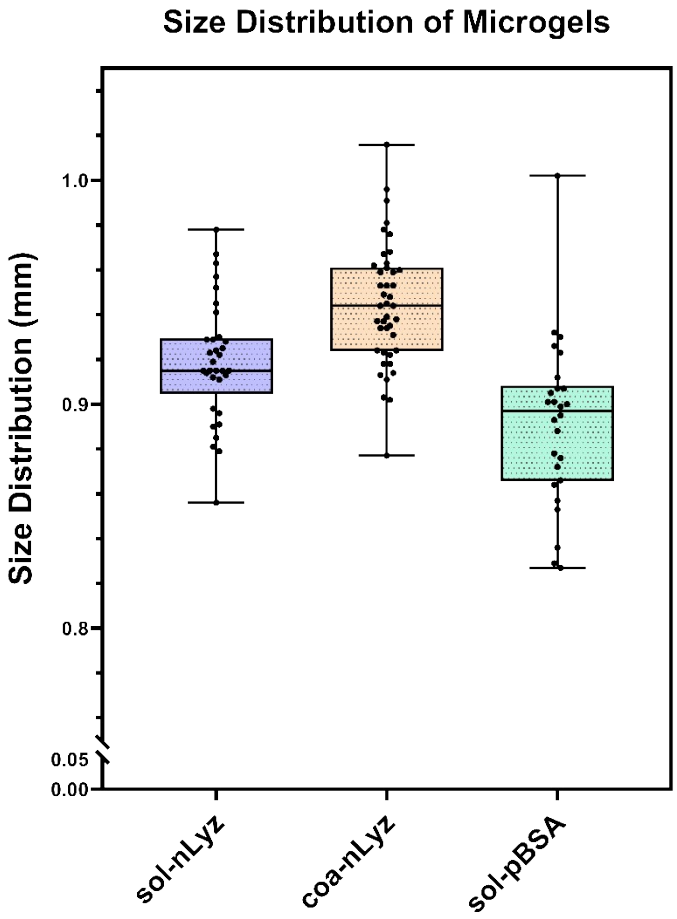

Figure S3D. Microgel size distribution of sol-nLyz, coa-nLyz, and sol-pBSA formulation. Statistically, the polydispersity index of each formulation was computed: $Đ_{sL}$ = 0.00848, $Đ_{cL}$ = 0. 00856, and $Đ_{sB}$ = 0. 00176.

S.2.3. In-droplet Mixing performance

As described in the main text, all 3 types of microgels were briefly characterized by the computation of mixing indices. The indicated diameter was chosen and the RGB profile along the diameter was extracted by ImageJ using the UV-fluorescent images as the following **Fig. S4A**, **S4B**, and **S4C** with labelled diameters indicating each extractable microgels of sol-nLyz, coa-nLyz, and sol-pBSA, respectively.

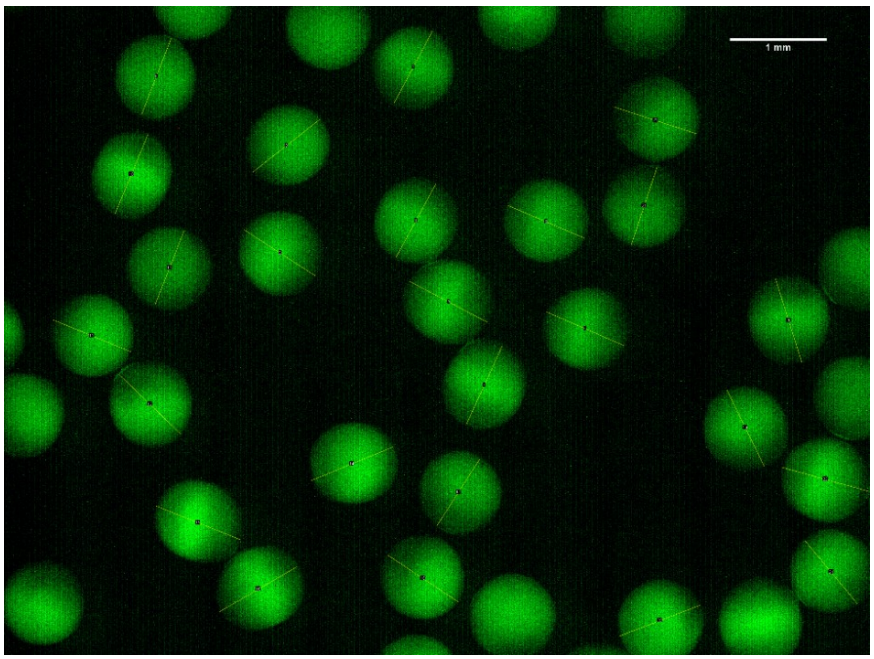

Figure S4A. Sample UV-fluorescent microscopic image of sampled sol-nLyz microgels processed for RGB-profile extraction. Yellow strikes indicate the manually chosen diameter for extraction.

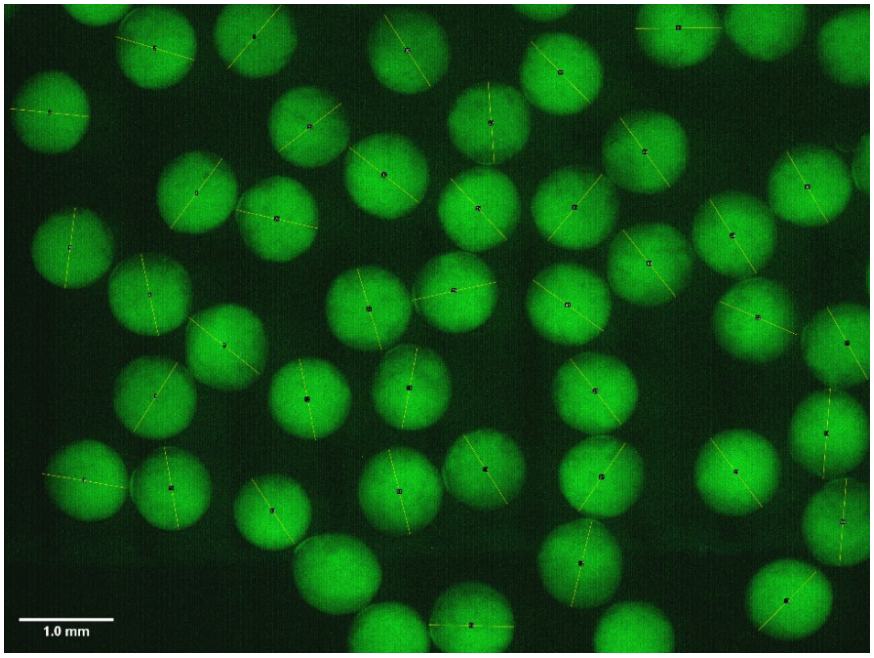

Figure S4B. Sample UV-fluorescent microscopic image of sampled coa-nLyz microgels processed for RGB-profile extraction. Yellow strikes indicate the manually chosen diameter for extraction.

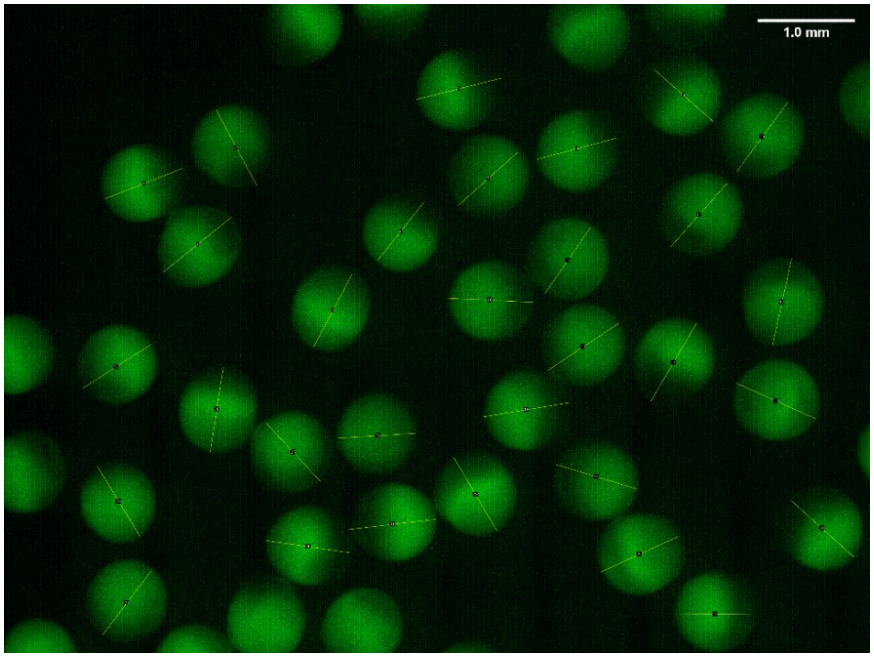

Figure S4C. Sample UV-fluorescent microscopic image of sampled sol-pBSA microgels processed for RGB-profile extraction. Yellow strikes indicate the manually chosen diameter for extraction.

For the data extraction and analysis of mixing index, we hereby use one measurement as an example, shown in the following **Fig. S4D**. The measurement was alongside the manually drawn symmetric axis on **Fig. S4D (a)**, and the RGB profile along this axis was extracted by ImageJ; upon extraction, the G-channel profile was screened with a moving mean with a window of 3-pixel using MATLAB (code is provided below), and plotted as **Fig. S4D (b)**. After the screening of the moving mean to damp the local noise, average and standard deviation of the G-intensity was evaluated and used to compute the mixing index of this measurement (as indicated on the plot). Lastly, summarizing all the measurements, **Fig. S4E** together with **Table S2** column 9 summarize the average mixing indices.

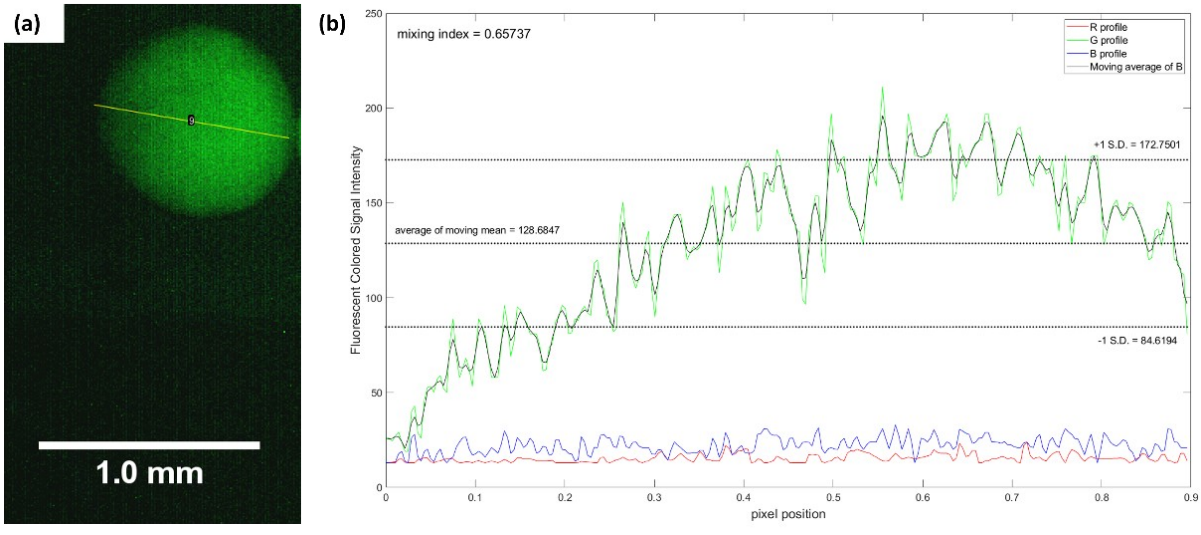

Figure S4D. (a) Assigned green-fluorescent signal symmetric axis over the diameter of a microgel. **(b).** Extracted RGB profile along the assigned symmetric axis, with a moving mean screened through the green-intensity signal.

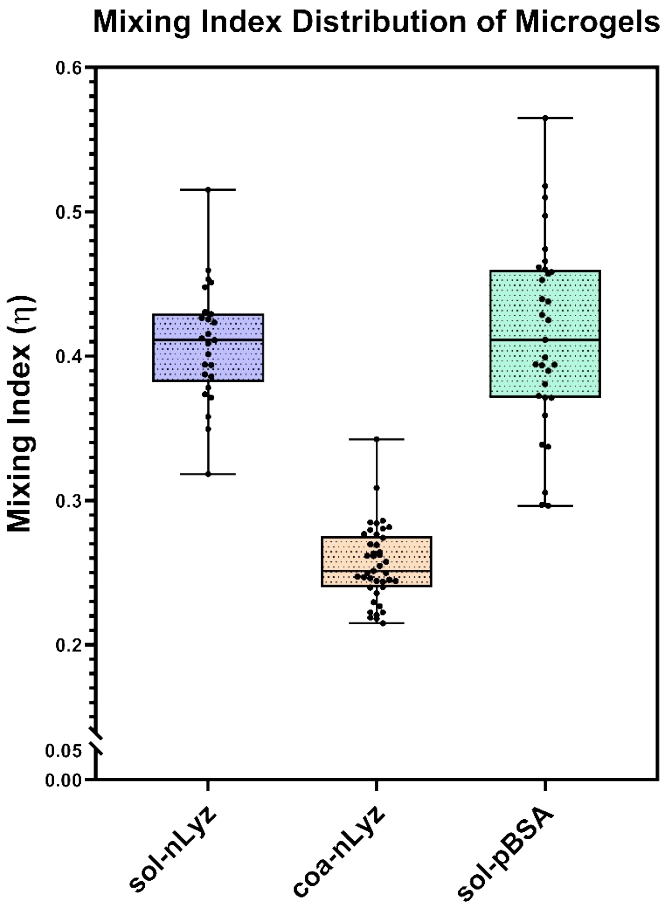

Figure S4E. Box plot of mixing indices of each formulation, with observation of that coa-nLyz having the relatively best in-droplet mixing performance while sol-nLyz and sol-pBSA showed similarity.

MATLAB Code of Mixing Index Calculator:

```
function [gAverage] = FluorMix(num, channel, window, analysisFileName)
%% Construct the filename matrix for reference
    % Generate a preset empty filename matrix to reduce operative memory
    csvNameMat = zeros(num,1);
    % Filling in the filename matrix with maximum number of labels.
    for i = 1:num
        csvNameMat(i,1) = i;
    end

%% Read the dataset for each item within the filename matrix
    % Generate preset empty averages and SD matrices to reduce operative memory
    AvgMat = zeros(num,1);
    StdMat = zeros(num,1);
    mixMat = zeros(num,1);
    % Data extraction of each file
    for j = 1:length(csvNameMat)
        % Add the csv. file suffix
        csvNameStr = [num2str(csvNameMat(j,1)),'.csv'];
        % Read the file
        RGBmat = readmatrix(csvNameStr);
        % Retrieve the pixel-axis of the dataset
        PP = RGBmat(:,1);
        P0 = PP(1);
        Pn = PP(length(PP));
        % Retrieve the RGB values of the dataset
        RR = RGBmat(:,2);
        GG = RGBmat(:,3);
        BB = RGBmat(:,4);
```

MATLAB Code of RGB Profile Plotter:

```
Function [mixPerc, GaccRange, Gmean, Gstd] = FluorPlotting(RGB_profile, window, alpha)

    RGBmat = readmatrix(RGB_profile);

    PP = RGBmat(:,1);
    P0 = PP(1); Pn = PP(length(PP));
    subp = linspace(P0,Pn);

    RR = RGBmat(:,2);
    GG = RGBmat(:,3);
    BB = RGBmat(:,4);

    MMR = movmean(RR,window);
    MMG = movmean(GG,window);
    MMB = movmean(BB,window);

    Gmean = mean(MMG);
    Gstd = std(MMG);

    GaccBot = Gmean - alpha .* Gstd;
    GaccTop = Gmean + alpha .* Gstd;
    GaccRange = ['[', num2str(GaccBot),',',num2str(GaccTop),']'];

    strMean = ['average of moving mean = ',num2str(Gmean)];
    strBot = ['lower acceptable limit = ',num2str(GaccBot)];
    strTop = ['upper acceptable limit = ',num2str(GaccTop)];

    mixPerc = (sum(MMG >= GaccBot & MMG <= GaccTop))./(size(MMG,1));

    strMix = ['mixed ratio = ',num2str(mixPerc)];

    figure()
    plot(PP,RR,'r-',PP,GG,'g-',PP,BB,'b-',PP,MMG,'k-',PP,Gmean,'k.',PP,GaccBot,'k.',PP,GaccTop,'k.');
    legend('R profile','G profile', 'B profile', 'Moving average of B');
    xlabel('pixel position');
    ylabel('Fluorescent Colored Signal Intensity');
    text(PP(length(PP)-30),(Gmean+2),strMean);
    text(PP(length(PP)-30),(GaccTop+2),strTop);
    text(PP(length(PP)-30),(GaccBot+2),strBot);
    text(PP(5),190,strMix);

end
```

S.2.4. Weighing of Microgels after Drying

As described in the main text, all 3 types of microgels were weighed to obtain a rough estimation of weight of microgel in dried state. **Table S2** column 10 summarize the average weight of dried microgels.

S.2.5. Swelling of each Formulation using Macrogel Counterparts

As described in the main text, swelling behavior of all 3 formulations were studied using macrogel counterparts due to physical difficulty to measure the volume of microgels and subsequent volumetric swelling ratio. Basically, this idealization was grounded in the assumption that the equilibrium swelling ratios, both volumetric and mass, of one type of microgels are identical to its macrogel counterpart (while the rate of swelling or the time required to reach equilibrium swollen state will be different). As a result, **Fig. S5** illustrates the swelling behavior of macrogels of a span of 168 hrs. The equilibrium swollen states were clearly observed after 36 hr of incubation for all 3 formulations. The equilibrium swollen states of both sol-nLyz and coa-nLyz were established after an initial hump of over-swelling around 2 to 12 hrs, while that of sol-pBSA were established without clear evidence of such initial hump. Furthermore, the swelling profiles suggested that the coa-nLyz formulation possessed a higher water absorption capacity compared to their sol-nLyz and sol-pBSA counterparts, respectively. Hypothetically, higher swelling capacity at equilibrium swollen state of coa-nLyz was obtained due to the existence of extra coacervating agents. As a summary, the mass swelling ratio from relaxed state to equilibrium swollen state ($Q_{r\rightarrow es}^{\ M}$) was averaged about the equilibrium swollen state (timepoint of 48 hr onwards) and enlisted in **Table. S2** column 11.

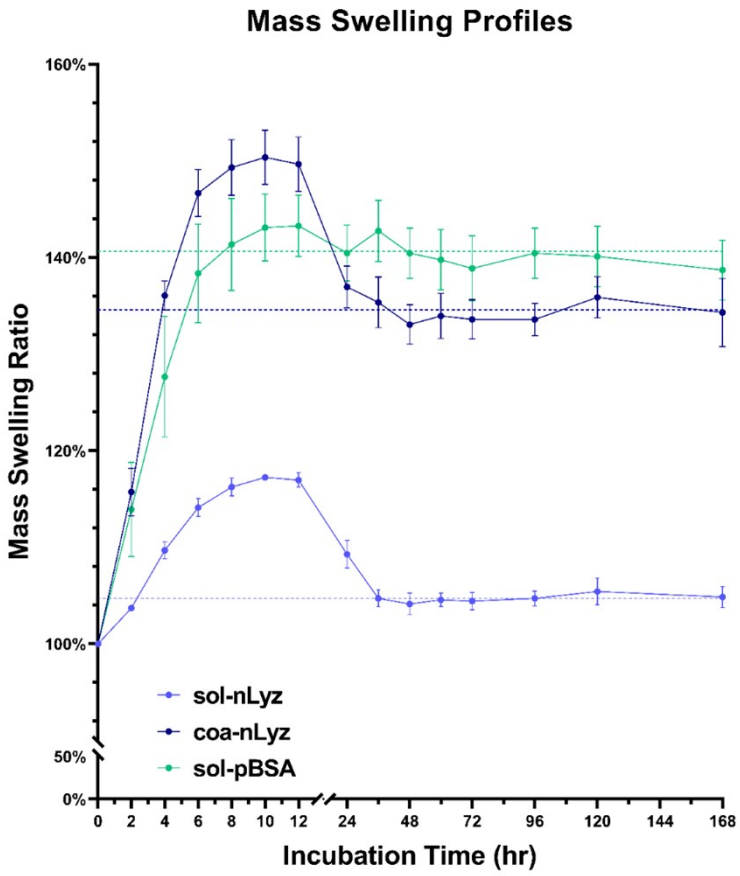

Figure S5. Relaxed to equilibrium-swollen state mass swelling profiles of all formulations, with horizontal dashed line indicating the averaged swelling ratio after reached equilibrium. The experiment setup modeled a pseudo-infinite sink condition, and n_{sample} = 3.

Next, to estimate the average mesh size at equilibrium swollen state, the overlapping concentration (c^*), and radius of gyration (R_g) of Dex_{40k} polymer are calculated based on following sequential of equations:

- **Mark-Houwink Correlation**

$$[\eta] = k_{MH}(M_w)^a \qquad \textbf{Eqn. S3A}$$

$[\eta] =$ intrinsic viscosity (dL/g)

$k_{MH} =$ Mark-Houwink coefficient (dL/g)

$a =$ Mark-Houwink exponent

For dextran aqueous solution under $T = 25$ ℃, Güner reported $k_{MH} = 7.337 \times 10^{-4}\ dL/g$ and $a = 0.533$, which represents water is roughly a theta solvent for dextran. [3] This leads to a resultant intrinsic viscosity of Dex40k under 25 ℃ as $0.208\ dL/g$.

- **Flory-Fox Equation**

$$R_g = \left(\frac{[\eta]M_w}{\Phi_0}\right)^{\frac{1}{3}}$$ **Eqn. S3B**

$R_g =$ radius of gyration (m)

$\Phi_0 \approx 2.1 \sim 2.5 \times 10^{23}\, mol^{-1} =$ Flory constant

For dextran aqueous solution under $T = 25$ ℃, given the theta solvent condition with flexible-chain polymer assumption, we choose $\Phi_0 = 2.1 \times 10^{23}\, mol^{-1}$ for calculation. [4] This leads to a resultant radius of gyration of Dex40k under 25 ℃ as $15.8\, nm$.

- **Graessley Equation**

$$c^* = \frac{6^{1.5} M_w}{N_A (2R_g)^3}$$ **Eqn. S3C**

$c^* =$ overlapping concentration (mg/mL)

$N_A = 6.022 \times 10^{23}\, mol^{-1} =$ Avogadro's number

By the previous steps, Graessley Equation derived from de Gennes theory [5] leads to a resultant overlapping concentration of Dex_{40k} under 25 ℃ as $30.9\, mg/mL$, which corresponds to $3.1\ w/v\%$.

Lastly, we adopted the Blob model mesh size estimation (**Eqn. S3D**) deduced from de Gennes theory to extract averaged mesh size at equilibrium swollen state for all four types of Dex40k-VS:SH microgels. [6]

$$\bar{\xi}_m = \left(Q_{r\to eq}^{\ V}\right)^{\frac{1}{3}} R_g \left(\frac{c}{c^*}\right)^{\frac{\nu}{1-3\nu}}$$ **Eqn. S3D**

$\bar{\xi}_{eq} =$ average mesh size at equilibrium swollen state of hydrogel (nm)

$Q_{r\to eq}^{\ V} =$ average volumetric swelling ratio from relaxed to equilibrium swollen state

$\nu =$ Flory's exponent

Ioan *et al.* reported the dextran aqueous solution possessing Flory's exponent value about 0.45 which was deduced from the branching structure of dextran polymer. [7], [8] Then, assuming the swollen hydrogels possess densities approximately equal to that of water, i.e., 1 g/cm^3, the average volumetric swelling ratio can be equivalent to the mass swelling ratio $Q_{r\to eq}^{\ M}$ given a cubic root of swelling ratio would further minimize this error. Following **Table S2** column 12 summarize the computed mesh size of each formulation.

S.2.6. Swelling of Blank Bulk Carrier Matrix

As described in the main text, swelling behavior of the chosen $tetraPEG_{20k}$-VS:SH bulk carrier matrix was investigated using an empty-loading formulation (only 2.5 w/v% $tetraPEG_{20k}$ polymer without any protein or excipient). The tested sample was initially measured $m_{gel} =$ 25 mg and $V_{gel} =$ 35 µL upon fabrication (at the relaxed state). As a result, **Fig. S6** illustrates the swelling behavior of the empty-loading bulk carrier matrix slab of a span of 240 hrs. The swelling behavior exhibited unusual deswelling property under physiological $1\times$ PBS condition, which was hypothetically due to the concentration of tetra-arm PEG selected for crosslinking was lower than its theoretical overlapping concentration. [9] Lastly, we adopted the theoretical model recently modified by Richbourg and Peppas for multi-armed PEG mesh sizing estimation (**Eqn. S4A, S4B, and S4C**) with

experimental swelling data.[10] As a result, the 2.5 w/v% tetraPEG$_{20k}$-VS:SH bulk carrier matrix yielded a roughly ~12.7 nm of mesh size as estimated.

$$\frac{1}{\overline{M}_c} = \frac{f}{f-2}\left[\frac{f}{M_w} - \frac{\ln(1-\varphi_{eq}) + \varphi_{eq} + \chi\cdot(\varphi_{eq})^2}{V_w\cdot\rho_{PEG}\cdot\left((\varphi_{eq})^{\frac{1}{3}} - \frac{1}{2}\varphi_{eq}\right)}\right] \quad \textbf{Eqn. S4A}$$

$\overline{M}_c =$ average molecular weight between adjacent crosslinking points

$f =$ number of functionalities (arms) of selected multi-armed PEG

$M_w =$ weight-average molecular weight of the PEG

$V_w = 18\ cm^3/mol =$ molar volume of water

$\rho_{PEG} = 1.125\ g/cm^3 =$ density of dry PEG

$\chi = 0.426 =$ Flory-Huggins solvent-polymer interaction parameter of PEG-water system [11]

$\varphi_{eq} =$ volumetric fraction of PEG at equilibrium swollen state

$$\varphi_{eq} = \frac{c}{\rho_{PEG}}\left[\frac{\rho_w V_{gel}}{\rho_w V_{gel} + m_{gel}\left(Q_{r\to eq}^{\ M} - 1\right)}\right] \quad \textbf{Eqn. S4B}$$

$c = 25\ mg/mL =$ experimental concentration of PEG

$\rho_w = 1\ g/mL =$ density of water

$m_{gel} = 25\ mg =$ initial mass of the sample at relaxed state

$V_{gel} = 35\ \mu L =$ initial volume of the sample at relaxed state

$Q_{r\to eq}^{\ M} =$ average mass swelling ratio from relaxed to equilibrium swollen state

$$\overline{\xi}_m = (\varphi_{eq})^{-\frac{1}{3}}\sqrt{\left(1-\frac{2}{f}\right)\frac{\lambda C_\infty L^2 \overline{M}_c}{M_r}} \quad \textbf{Eqn. S4C}$$

$\lambda = 3 =$ backbone factor of PEG [10]

$C_\infty = 6.9 =$ infinite chain-length characteristic ratio of PEG [10]

$L = 0.154\ nm =$ number-average covalent bond length of PEG in one repeating unit [10]

$M_r = 44\ Da =$ molecular weight of one PEG repeating unit

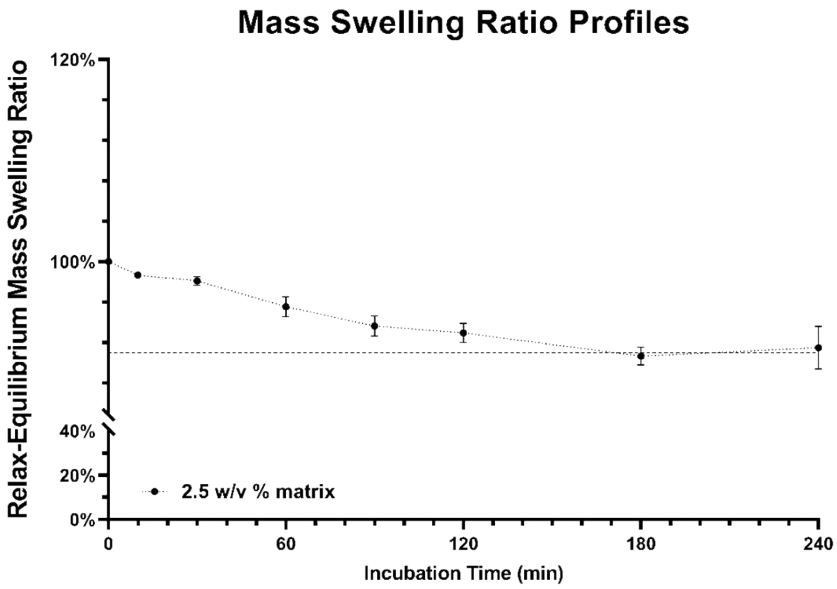

Figure S6. Mass swelling profile of 2.5 w/v% tetraPEG$_{20k}$-VS:SH bulk carrier matrix within a studied timespan of 240 hr. Dashed lines indicate the calculated mass swelling ratio from relaxed state to the equilibrium swollen state (91%). The experiment setup modeled a stagnant batch condition, and n_{sample} = 3.

S.2.7. Scanning Electron Microscopy (SEM) Images

SEM images were taken to provide additional visualization of the microscopic structure of the surface of dried microgels post-fabrication and the cross-section cut of MHC after release study. The following **Fig. S7A** shows SEM images of some dried (antisolvent by isopropanol during cleaning right after fabrication) sol-nLyz microgels (left) and a zoomed-in image of one of the microgels (right); the **Fig. S7B** shows SEM image of the cross-sectional cut surface of a pure sol-nLyz loaded MHC slab; the **Fig. S7C** shows SEM images that zoomed in to observe the crystals – hypothetically, white, flaky crystals of salt and dark, chunky crystals of lysozyme.

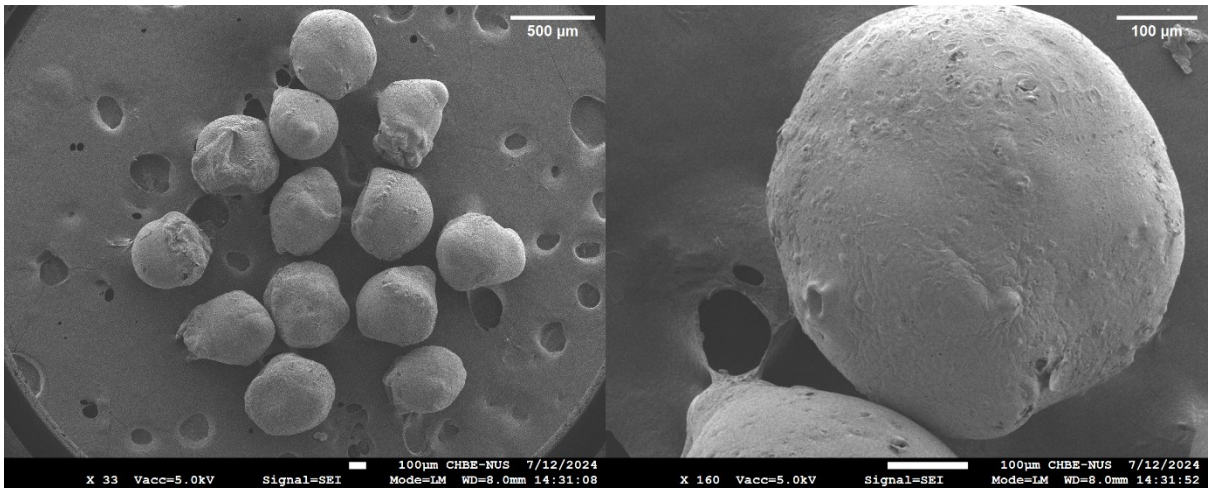

Figure S7A. SEM image of a cluster of dried, post-fabrication sol-nLyz microgels (left) and a zoomed-in image of one of the microgels. The non-spherical, deformed morphology is an artifact of the drying process during SEM sample preparation.

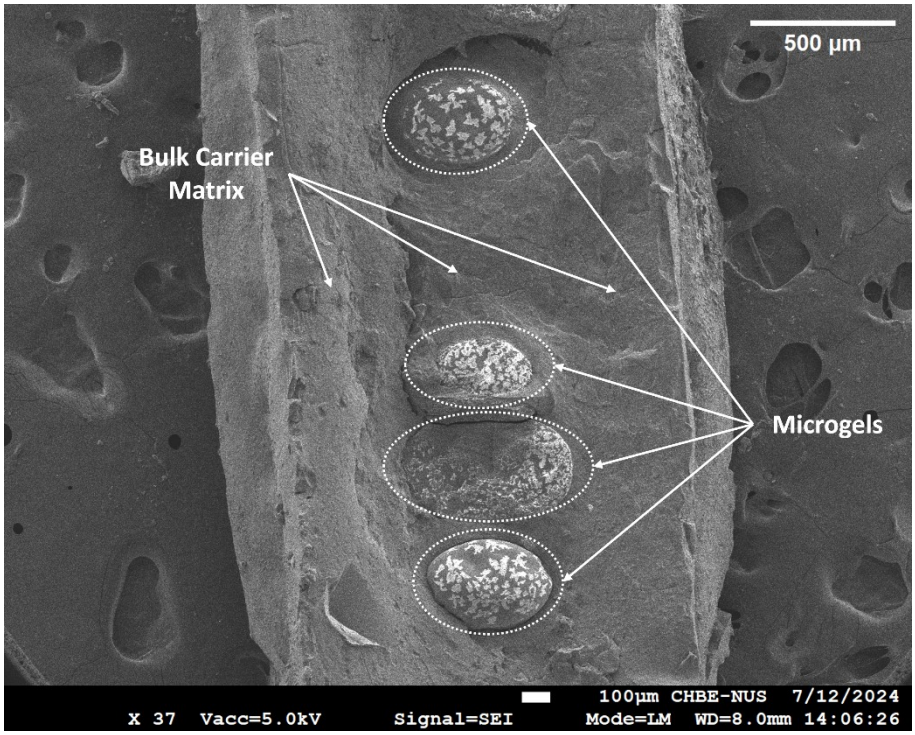

Figure S7B. SEM image of the cross-section of an MHC slab (purely sol-nLyz microgels embedded). The image indicates the three-layer structure of the slab: top and bottom layer of bulk carrier matrix and a center layer of microgels embedded in and surrounded by the bulk carrier matrix.

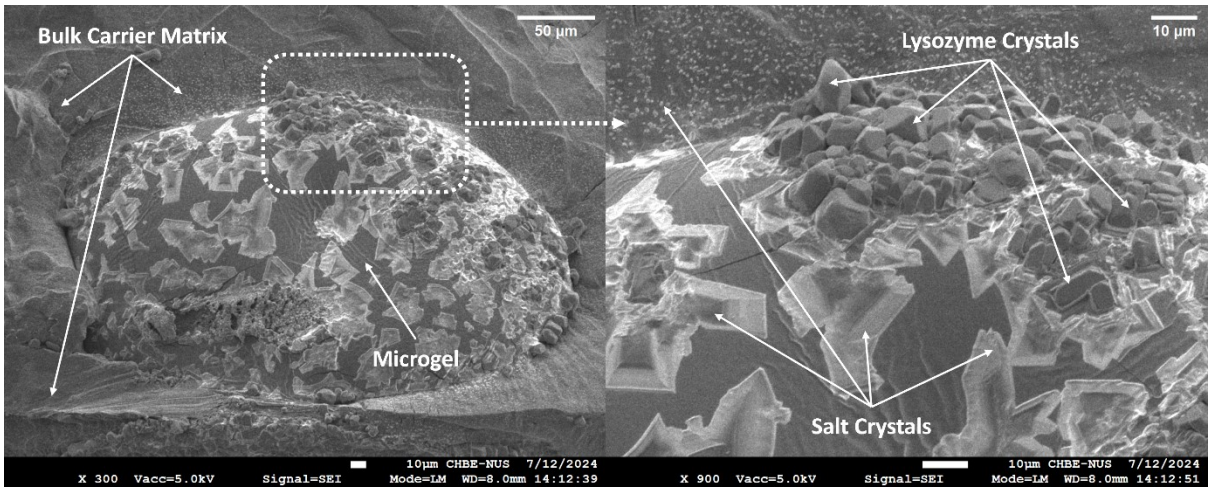

Figure S7C. SEM images zoomed in to one of the microgels (sol-nLyz) embedded in the MHC (left) and a further zoomed image to observe the flaky salt crystals and rhombus-like lysozyme crystals formed on the microgel surface due to the extensive drying of a swollen sample (right). Additionally, the right image also showed white spots of salt crystals, much smaller in size, formed in the bulk carrier matrix. All crystals formed were artifacts of the extensive drying process during SEM sample preparation.

S.3. Assay Standard Curves

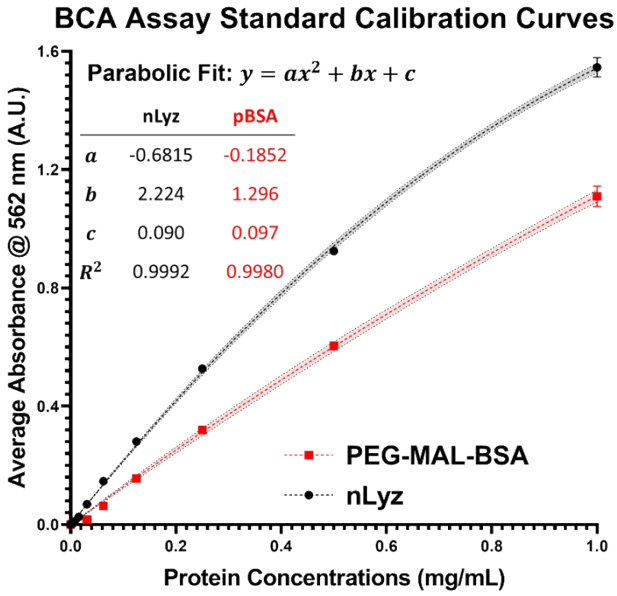

Figure S8A. Standard curves of BCA Assay for native hen egg white lysozyme (nLyz) and PEGylated bovine serum albumin (PEG-MAL-BSA or pBSA). The BCA Assay was completed following the protocol provided by ThermoFischer (supplier).

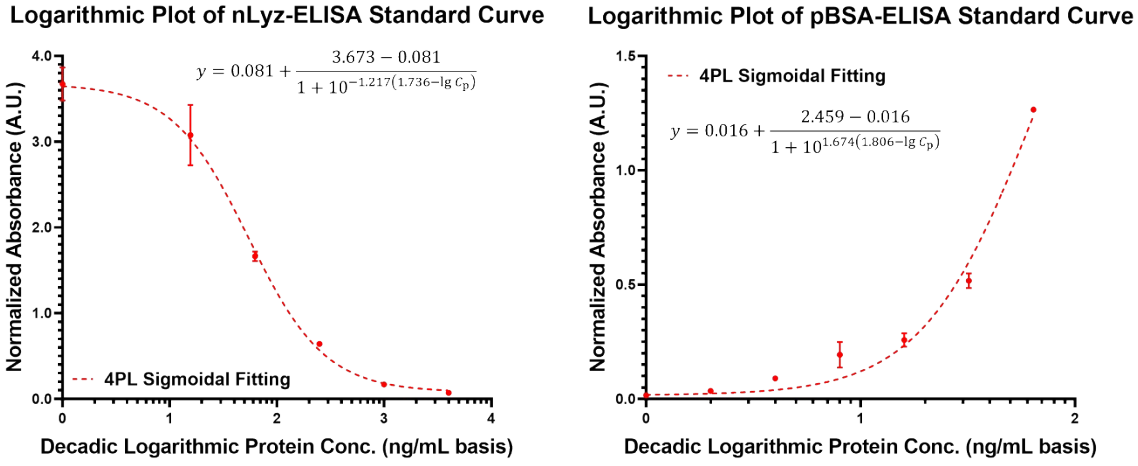

Figure S8B. Standard curves of ELISA Assays for native hen egg white lysozyme (nLyz) and PEGylated bovine serum albumin (PEG-MAL-BSA or pBSA), respectively. The competitive ELISA Assay for nLyz was completed following the protocol provided by Novus Biologicals (supplier), while the direct ELISA assay for BSA was completed following the protocol provided by Cygnus Technologies (supplier).

Table. S2. Summary of Compositions and Characterizations of 4 Designed Formulations

Formulation	**Stream Dex-VS** (Solution X)		**Stream Dex-SH + Prot.** (Solution Y)		**Conditioning Buffer Stream** (Solution Z)	t_{gel} (sec)	d_j (μm)	$\overline{\eta}_j$	m_{bead}° (μg)	$Q_{r\to es}^{M}$	$\overline{\xi}_m$ (nm)
sol-nLyz	Dex_{40k}-$VS_{5\%}$	$9.96 w/v\%$	Dex_{40k}-SO_2-$TTSH_{5\%}$	$13.19 w/v\%$	3x PBS + $600\ \mu g/mL$ NaN_3	439	$919.2 \pm$	0.409 ± 0	83.3 ± 5.7	$\sim 105\ \%$	4.7
	Dex_{40k}-$FITC_{1\%}$-$VS_{6\%}$	$0.87 w/v\%$	nLyz	$15\ mg/mL$							
coa-nLyz	Dex_{40k}-$VS_{5\%}$	$9.96 w/v\%$	Dex_{40k}-SO_2-$TTSH_{5\%}$	$13.19 w/v\%$	3x PBS + $600\ \mu g/mL$ NaN_3	400	$944.3 \pm$	0.256 ± 0	50.5 ± 2.6	$\sim 135\ \%$	5.1
	Dex_{40k}-$FITC_{1\%}$-$VS_{6\%}$	$0.87 w/v\%$	nLyz	$15\ mg/mL$							
	Dex_{40k}-SO_3^- Na^+	$15\ mg/mL$									
sol-pBSA	Dex_{40k}-$VS_{5\%}$	$9.96 w/v\%$	Dex_{40k}-SO_2-$TTSH_{5\%}$	$13.19 w/v\%$	3x PBS + $600\ \mu g/mL$ NaN_3	608	$891.5 \pm$	0.415 ± 0	48.5 ± 6.4	$\sim 141\ \%$	5.2
	Dex_{40k}-$FITC_{1\%}$-$VS_{6\%}$	$0.87 w/v\%$	$mPEG_{2k}$-MALS-BSA	$15\ mg/mL$							

Reference

[1] Yu Y, Chau Y. One-step “click” method for generating vinyl sulfone groups on hydroxyl-containing water-soluble polymers. *Biomacromolecules*. 2012 Mar 12;13(3):937-42.

[2] Lau CML, Jahanmir G, Yu Y, Chau Y. Controllable multi-phase protein release from in-situ hydrolyzable hydrogel. *Journal of Controlled Release*. 2021 Jul 10;335:75-85.

[3] Güner A. Unperturbed dimensions and the theta temperature of dextran in aqueous solutions. *Journal of Applied Polymer Science*. 1999 May 16;72(7):871-6.

[4] Masuelli MA. Dextrans in aqueous solution. Experimental review on intrinsic viscosity measurements and temperature effects. *Journal of Polymer and Biopolymer Physics and Chemistry*. 2013 Nov 22;1(1):13-21.

[5] Graessley WW. Polymer chain dimensions and the dependence of viscoelastic properties on concentration, molecular weight and solvent power. *Polymer*. 1980 Mar 1;21(3):258-62.

[6] Yu Y, Chau Y. Formulation of in situ chemically cross-linked hydrogel depots for protein release: from the blob model perspective. *Biomacromolecules*. 2015 Jan 12;16(1):56-65.

[7] Antoniou E, Tsianou M. Solution properties of dextran in water and in formamide. *Journal of Applied Polymer Science*. 2012 Aug 5;125(3):1681-92.

[8] Ioan CE, Aberle T, Burchard W. Structure properties of dextran. 2. Dilute solution. *Macromolecules*. 2000 Jul 25;33(15):5730-9.

[9] Liu W, Gong X, Zhu Y, Wang J, Ngai T, Wu C. Probing sol–gel matrices and dynamics of star PEG hydrogels near overlap concentration. *Macromolecules*. 2019 Nov 13;52(22):8956-66.

[10] Richbourg NR, Peppas NA. The swollen polymer network hypothesis: Quantitative models of hydrogel swelling, stiffness, and solute transport. *Progress in Polymer Science*. 2020 Jun 1;105:101243.

[11] Merrill EW, Dennison KA, Sung C. Partitioning and diffusion of solutes in hydrogels of poly (ethylene oxide). *Biomaterials*. 1993 Jan 1;14(15):1117-26.